Evaluation of Precipitation Retrievals From Orbital Data Products of TRMM Over a Subtropical Basin in India

J. Indu and D. Nagesh Kumar

***Abstract*—The spatial error structure of daily precipitation derived from the latest version 7 (v7) tropical rainfall measuring mission (TRMM) level 2 data products are studied through comparison with the Asian precipitation highly resolved observational data integration toward evaluation of the water resources (APHRODITE) data over a subtropical region of the Indian subcontinent for the seasonal rainfall over 6 years from June 2002 to September 2007. The data products examined include v7 data from the TRMM radiometer Microwave Imager (TMI) and radar precipitation radar (PR), namely, 2A12, 2A25, and 2B31 (combined data from PR and TMI). The spatial distribution of uncertainty from these data products were quantified based on performance metrics derived from the contingency table. For the seasonal daily precipitation over a subtropical basin in India, the data product of 2A12 showed greater skill in detecting and quantifying the volume of rainfall when compared with the 2A25 and 2B31 data products. Error characterization using various error models revealed that random errors from multiplicative error models were homoscedastic and that they better represented rainfall estimates from 2A12 algorithm. Error decomposition techniques performed to disentangle systematic and random errors verify that the multiplicative error model representing rainfall from 2A12 algorithm successfully estimated a greater percentage of systematic error than 2A25 or 2B31 algorithms. Results verify that although the radiometer derived 2A12 rainfall data is known to suffer from many sources of uncertainties, spatial analysis over the case study region of India testifies that the 2A12 rainfall estimates are in a very good agreement with the reference estimates for the data period considered.**

***Index Terms*—Asian Precipitation Highly Resolved Observational Data Integration Toward Evaluation of the Water Resources (APHRODITE), basin, orbital, precipitation, Tropical Rainfall Measuring Mission (TRMM), uncertainty.**

I. Introduction

OVER the past two and half decades, satellite-based precipitation estimates from Microwave Remote Sensing (MRS) have exhibited tremendous progress proving to be a reliable source for quantitative estimation of precipitation from space [1]–[8]. However, along with the widespread acceptance of these products, it has also been recognized that they contain large uncertainties. Uncertainty evaluation studies focus on either the accuracy of rainfall accumulated over time (e.g., season/year) or the evaluation of rainfall intensities from microwave-based satellite orbital data products (hereinafter used synonymously with orbital products). Fewer studies have been directed toward the objective of evaluating the rainfall from the orbital data products. The error components of orbital data products interact nonlinearly with hydrologic modeling uncertainty [9], [10]. These products are known to potentially cause large uncertainties during real time flood forecasting studies at the watershed scale because the highly varying land surface emissivity offers a myriad of complications hindering accurate rainfall estimation over land regions. The dependence of land surface emissivity on physical temperature, vegetation, soil moisture, etc., and its spatio-temporal variability makes it necessary to rely on microwave high-frequency channels, which are less sensitive to cloud water than the low-frequency channels.

Knowledge regarding the uncertainty contribution from orbital data products enables the data developers to improve the performance of their algorithms and data users to assess model simulation outputs that result in more reliable prediction. Despite the efforts in developing finer scale products from MRS, obtaining precipitation at the required accuracy for basin scale hydrology still remains a challenge [11], [12]. In order to broaden the application of orbital products at relevant spatio-temporal scales, a thorough investigation regarding the nature and magnitude of errors is essential.

There are many data products publicly made available from MRS [1], [6], [13] at a global scale, which are potentially helpful for many scientific investigations and applications [12], [14]–[19]. Among these, data from the microwave sensors onboard the low earth orbiting satellite of the Tropical Rainfall Measuring Mission (TRMM), launched in 1997, have revolutionized the global view of precipitation. TRMM studies rainfall variability in the tropics using a collocated suite of instruments, namely, the passive TRMM Microwave Imager (TMI) and the active precipitation radar (PR). During its mission lifetime, rainfall retrieval algorithms based on TMI and PR have provided an enormous volume of tropical rainfall data [20]–[23]. The standard level 2 data products of TRMM made available by the NASA Goddard Space Flight Center (GSFC), support rainfall rates estimated either using TMI (the 2A12 product) or PR (the 2A25 product) or a combination of both (the 2B31 product). Prior to the launch of TRMM, Wilheit [24] proposed an error model ascertaining that the total error in climatological precipitation is mainly due to sampling

Manuscript received July 8, 2014; revised November 6, 2014, January 12, 2015, April 9, 2015, and May 13, 2015; accepted May 23, 2015. The work of D. N. Kumar was supported by the Ministry of Earth Sciences, Government of India, through Project No. MoES/ATMOS/PP-IX/09.

J. Indu is with the Department of Civil Engineering, Indian Institute of Science, Bangalore 560 012, India and also with Department of Civil Engineering, Indian Institute of Technology Bombay, Mumbai 400 076, India.

D. Nagesh Kumar is with the Department of Civil Engineering, Indian Institute of Science, Bangalore 560 012, India, and also with the Centre for Earth Sciences, Indian Institute of Science, Bangalore 560 012, India.

Color versions of one or more of the figures in this paper are available online at http://ieeexplore.ieee.org.

Digital Object Identifier 10.1109/TGRS.2015.2440338

errors, random instrument errors and correlated algorithmic errors. Their study also emphasized that although sampling and retrieval errors occur independently, these get entangled during statistical integration of monthly/seasonal rainfall produced from TRMM orbital data. Some of the prominent studies related to uncertainty assessment of TRMM orbital data products are discussed here.

Most of the studies on TRMM level 2 data products have used the previous versions, namely, version 5 (v5) and version 6 (v6) data for comparison. Some of the prominent studies comparing both rainfall products are summarized in the following. Kummerow *et al.* [25] using v5 data have reported a difference between TMI and PR rainfall intensities, which amounted to 20% over land and ∼23% over oceans. Masunaga *et al.* [26] investigated the regional trends in hydrometeor profiles derived from TMI 2A12 (hereinafter referred to as 2A12) and PR 2A25 (hereinafter referred to as 2A25) algorithms and concluded that 2A25 underestimates the precipitation water profiles in the tropics. Furthermore, they also stated that a disagreement between both rainfall products results due to different physical principles underlying both TMI and PR measurements coupled with algorithmic bias, which occurs during conversion of precipitation water to rainfall rate.

Nesbitt *et al.* [27] evaluated rainfall estimates from v5 2A25 and 2A12 products over the tropics. Their study revealed that accounting the regime-dependent biases lead to reduction in systematic bias within a microwave-based precipitation algorithm. Sanderson *et al.* [28] evaluated the effect of spatial and temporally dependent algorithm biases on diurnal rainfall cycle using v5 rainfall from 2A12, 2A25, and 2B31. Wolff and Fisher [29] evaluated v6 2A25 and 2A12 products for the land, ocean and coastline over the TRMM Ground Validation sites and reported the underestimation by 2A25 v6 over land regions particularly when rain rates were greater than 10–20 mm/hr. Studies by Amitai *et al.* [30] have made a similar conclusion after comparing 2A25 v6 algorithm to National Oceanic and Atmospheric Administration Next-Generation Quantitative Precipitation Estimate product.

Some studies have generated high-resolution climatologies for use in rainfall-land-surface interactions based on 2A25 and 2B31 data products [31]–[35]. This includes the TRMM 3G68 data product, which consist of rainfall retrievals averaged in space over $0.5^\circ \times 0.5^\circ$ grid boxes. The 3G68 product contains the 2A12, 2A25, and 2B31 rainfall rates averaged over space but not in time. Bowmann *et al.* [34] have used the TRMM 3G68 data product with *in situ* measurements using rain gauges on the NOAA TAO/TRITON buoy array in the tropical Pacific. Their study revealed that the TMI derived rainfall have near zero bias with respect to the buoy rain gauges in comparison with the PR-derived rainfall, which exhibited about 30% low bias relative to the gauge measurements. Studies by Kikuchi and Wang [36] have examined the diurnal variations of global tropical precipitation using the TRMM 3B42 and 3G68 data.

The inconsistencies of 2A12 (v6) land rainfall estimation were summarized by Wang *et al.* [37]. Their study has envisioned improvements for v7 2A12 algorithm, which forms the basis for the Global Precipitation Measurement (GPM) Global Microwave Imager algorithm. Studies by Gopalan *et al.* [38] highlighted improvements in the v7 2A12 algorithm by proving that addition of a more comprehensive set of TMI-PR collocations improved the 2A12 rain rates on a global scale but regional biases still remain owing to warm rainfall, lack of appropriate surface screening, etc. Recent studies by Zagrodnik and Jiang [39] have compared v6 and v7 rainfall estimates from the 2A25 and 2A12 products with respect to the Next Generation Weather Radar (NEXRAD) Multisensor Precipitation Estimate stage-IV hourly rainfall product. Their studies, based on detailed statistical analysis conducted for $1/7^\circ \times 1/7^\circ$ grids over the U.S., examined the influence of v7 TRMM rainfall algorithms on rainfall retrievals relative to ground reference data. All these studies indicate that although substantial improvements have been achieved in estimation of rainfall estimates using PR and TMI, significant biases still exist. The biases exhibited by TRMM orbital products can contribute to a still higher level of uncertainty when analyzed over smaller space-time scales.

Keeping these in mind, the present work investigates the performance of TRMM level 2 data products over the Indian subcontinent after gridding them to a space scale of $1^\circ \times 1^\circ$ and time scale of 1 day. The Indian summer monsoonal rainfall spanning over June, July, August, and September (JJAS) months forms an integral part of the South Asian monsoon, which plays a major role in global water cycle. Most parts of India receive a significant portion of total annual rainfall during the JJAS months. Hence, this paper utilizes a 6-year data period (from June 2002 to September 2007) of TRMM seasonal rainfall from the v7 orbital data products of 2A12, 2A25 and 2B31 over India. Only post 2001 data products are considered for analysis owing to the TRMM orbital boost from 350 to 402.5 km in August 2001, which altered the data quality significantly.

This work is driven by the need to understand the uncertainty of TRMM rainfall over regional scales in order to make the study directly relevant to data product developers engaged in improving their algorithms for follow-up missions such as Global Precipitation Mission (GPM) [40]. Section II summarizes various data products employed in the present study. The relative merits of radar and radiometer derived rainfall estimates are briefly discussed in Section III. The methodology employed for this paper is described briefly in Section IV. Section V presents the results of preliminary analysis conducted to finalize the case study region in India. Performance evaluation of the three level 2 data products over the case study region are discussed using metrics derived from the contingency table. This section also discusses results of error characterization employed using various error models, followed by error decomposition technique to disentangle the total bias into their systematic and random components. Section VI summarizes the major conclusions of this paper followed by the final remarks.

II. Data

The TRMM data systems were designed to develop rainfall products, error budgets, 3-D vertical precipitation structure, latent heat profiles, etc. (to name a few), with an aim to minimize the set of products that satisfied the mission requirements. These data products are made available in levels 1, 2, and 3

as per the standard NASA nomenclature. A comprehensive discussion of all the TRMM rainfall products is well beyond the scope of this paper. An overview of the level 2 algorithms that were deemed to play an instrumental role to the TRMM mission's success is presented in this paper. As the intent of this paper is to evaluate the performance of precipitation estimates from TRMM data products obtained using TMI and PR, the present study uses level 2 data products namely, the PR-derived 2A25 [41]–[44], TMI derived 2A12 [4], [37], [43] and the combined PR-TMI based 2B31data [45]–[50]. A brief description regarding the data products employed for the present study is summarized here.

A. TMI 2A12 Data

The TMI 2A12 product developed using the Goddard profiling algorithm (GPROF) [25], estimates hydrometeor (precipitation sized particles) profiles by matching the observed passive microwave brightness temperatures (Tb) with those from a pre existing database of simulated hydrometeor profiles using the Bayesian inversion scheme [4], [5]. This database computed using cloud-resolving models such as Goddard Cumulus Ensemble Model are tested well for tropical convective systems [4]. Over land, the 2A12 algorithm mainly relies on ice scattering frequencies (such as 85 GHz) for rainfall estimation, which incorporates uncertainty because of the empirical relationship used to relate ice-scattering optical depth aloft and the rain rate underlying the atmospheric ice layer [51]–[53].

B. PR 2A25 Data

The observations from PR enable a comparatively more direct measurement of rainfall rate than TMI. Rainfall estimates from 2A25 are calculated by the Hitschfeld–Bordan method [42] and the surface reference technique [48]. The 2A25 "PR Profile" produces the vertical rainfall rate profile for each radar beam at each resolution cell of the PR radar along with the attenuation corrected radar reflectivity (Z) profile. This data product contains the derived rainfall and reflectivity information as calculated by the PR rainfall processing algorithm. For this paper, the PR-derived near-surface rainfall (NSR) is used. This represents the rainfall rate near the surface within a range of 0 to 3000 mm/hr. As radar echoes from near the surface will usually be contaminated by the main lobe clutter, NSR represents the lowest point in the clutter free region for each angle bin.

C. Combined PR-TMI 2B31 Data

The guiding principle in the design of the 2B31 combined algorithm has always been to merge the information from both TMI and PR sensors into a single retrieval, which embodies the strengths of each sensor [53]. The 2B31 combined algorithm is entirely based upon a Bayesian retrieval technique, which matches observed radiances to a highly likely radar-rain profile and drop size distribution (DSD) [46]. The 2B31 algorithm utilizes radar reflectivity to estimate rain profile, constraining the estimation to be consistent with the total attenuation from TMI 10.65-GHz channel. To account for this constraint, the problem is expressed in terms of DSD. The expected value of Tb is generated using the resulting rainfall estimates. This value of Tb is compared with the measurements from passive microwave measurements to arrive at the most probable value for the DSD shape parameter [54].

D. TMPA

The TRMM Multisatellite Precipitation Analysis (TMPA) also known as TRMM 3B42 is a merged data product extensively used by scientists and researchers for various hydrometeorological and climatological applications and for studies related to uncertainty analysis over land and oceans. A number of attempts have been made in the last few years to validate this precipitation product at regional scales over land [55]–[69]. These studies provide information that a major hindrance in the usefulness of TRMM products is inefficient characterization of their inherent error structure. For the present study, the 3B42 data product is utilized for preliminary investigation to select the case study region within India.

E. APHRODITE Data

This is a high-resolution daily rainfall data set developed for the Asian region as part of the Asian Precipitation Highly Resolved Observational Data Integration Towards Evaluation of the Water Resources (APHRODITE) project. Details regarding the underlying algorithm and the data set are discussed in Xie *et al.* [69] and Yatagai *et al.* [70]. APHRODITE rainfall products are extensively being used for validating high-resolution climate model simulations [70] as well as for statistical downscaling of climate simulation outputs [71]. Studies by Yatagai *et al.* [72] have relied on APHRODITE rainfall data products for adjusting the TRMM-derived 3B43 rainfall data product, which is a 0.25° monthly precipitation product that merges the daily 3B42 precipitation data with the rain gauge information from the Global Precipitation Climatology Centre (GPCC) based on the technique by Huffman *et al.* [73], [74]. Use of a substantial rain gauge data and interpolation technique capable of including orographic effects makes these data products reliable. Previous studies comparing daily rainfall estimates from APHRODITE with those from the Indian Meteorological Department's rain gauges have indicated a very high correlation. Furthermore, a quantitative analysis of this product over India yielded a difference of less than 3 mm/day [75]. This makes it a reliable product to use for validation of satellite-derived precipitation estimates. Hence, for the present study, the APHRODITE monsoon Asia (MA) data product, which has a temporal resolution of 1 day and spatial resolution of $0.25^\circ \times 0.25^\circ$, is utilized as reference rainfall for evaluating the performance of TRMM rainfall estimates from 2A12, 2A25, and 2B31.

III. Relative Merits of TRMM Products

The standard TRMM data products provided by NASA GSFC include rainfall estimates derived either from TMI or PR or from their combined use. One of the major problems that need to be resolved to achieve the scientific goals of TRMM is to reduce the discrepancies among these rainfall products. The reasons for disagreement among these rainfall products can be attributed to a number of possible causes, some of which are briefly discussed in the following. As the 2A12 product (from radiometer TMI) and 2A25 (from radar PR) are based on different sensors, some of the plausible reasons for uncertainty

in rainfall detection would depend on the properties of these sensors along with the properties of seasonal rainfall occurring over the basin. For example, the 2A25 algorithm is known to suffer from low sensitivity toward weak rain and drizzle, which commonly occur due to shallow cumulus and stratiform clouds. This is owing to the wavelength and effective signal-to-noise ratio of PR [76]. The frequency of occurrence of isolated rainfall systems exhibits significant regional variability and the 2A12 algorithm is known to be weak in detecting such systems.

Another major factor contributing to TRMM rainfall uncertainty is the time-space sampling error. The TMI data swath of 878 km enables a better overview of the synoptic rainfall events than the PR (data swath of only 247 km). The wider TMI swath enables greater number of observations to be available for each spatial domain (grid box). This implies that since TRMM takes around 46 days to revisit an area approximately at the same local time, the resulting bias in average daily rainfall will be less in the 2A12 algorithm due to availability of greater number of observations during different times of the day. The TRMM radiometer has a sampling frequency of 1 every 15 h as compared with that of TRMM radar providing 1 sample every 50 h (depending upon the latitude of the sample). As a consequence, the PR-derived 2A25 algorithm will suffer from a comparatively greater sampling uncertainty than 2A12 algorithm thereby resulting in a greater bias in the 2A25 estimated rainfall [42], [77]. This implies that the sampling errors contributed by these data products are significant enough to make the apparent errors in the orbital rain rates significantly different from what they should be.

On the other hand, rainfall retrievals from the 2A25 algorithm rely on a direct measurement of reflectivity, which gives the 3-D structure of precipitation. In comparison, the 2A12 algorithm depends on radiometric measurements, which are more complicated and less direct since the Tb can be cluttered by surface emission depending on microwave frequency channel used and the fact that they represent cloud water and cloud ice rather than the hydrometeors near ground level. The 2A12 algorithm database computed from cloud-resolving models is known to be well tested for tropical convective systems. The process of deep convection usually results in lifting of water vapor to higher levels of atmosphere which condense into liquid water and freeze. The presence of atmospheric ice/solid precipitation above freezing level causes scattering of microwave radiation at higher frequency, thereby causing a decrease in the observed Tb. The radiometer (TMI) and radar (PR) have different sensitivities to atmospheric ice particles. The greater dielectric property of liquid water (four times) when compared with ice in the Rayleigh backscattering cross section accounts for the insensitivity of PR to small ice particles (unless these are large enough to be detected by 2.2 cm wavelength microwaves) in comparison with TMI, which is sensitive to even smaller ice hydrometeors owing to its high-frequency channels. Hence, PR tends to underestimate higher intensity rainfall over land owing to attenuation errors [26], [42]. This contributes a large discrepancy in the estimated amount of atmospheric ice.

Uncertainties are also being contributed by the underlying model assumptions used to estimate rainfall from both these algorithms (for example, treatment of DSD associated with individual retrieval algorithms). While the 2A25 algorithm assumes a gamma distribution for the DSD model to arrive at the reflectivity–rainrate (Z–R) relations, the 2A12 algorithms relies on a Marshall–Palmer DSD [42]. The uncertainties in the DSD assumptions are not critical for TMI measurements as Tb of low-frequency channels are relatively insensitive to DSD. In contrast to this, DSD assumptions more strongly affect the 2A25 algorithm as the radar reflectivity factor (Z) is the sixth moment of the DSD [26], [42].

TABLE I
LAYOUT OF CONTINGENCY TABLE

	Rain detected by reference (Yes)	No rain detected by reference (No)
Rain detected by TRMM orbital data (Yes)	Hit (H)	False (F)
No rain detected by TRMM orbital data (No)	Miss (M)	Null event (T)

One of the major challenges in hydrological applications is to characterize the error inherent in rainfall estimates from TRMM orbital data on a daily time scale for the JJAS months. Adequate consideration should be given to the uncertainties in these data sets prior to utilizing them in hydrologic and climatic studies.

IV. METHODOLOGY

The purpose of this paper is to evaluate the uncertainty in daily gridded rainfall estimates from TRMM orbital data during the JJAS months over regions of the Indian subcontinent subjected to poor detection of higher quantiles of rainfall by TMPA. A comparative evaluation of TMPA precipitation products is conducted with respect to APHRODITE data (as reference) for the overall monsoonal rainfall and their higher quantiles occurring over India during the 6-year monsoonal period (from June 2002 to September 2007). Performance evaluation was conducted based on metrics derived from the contingency table. Details regarding the performance metrics and error characterization are explained in the following.

A. Performance Metrics

The categorical indices from the contingency table (Table I) are extensively used in evaluation studies to validate the relationship between two categorical variables. While the contingency table metrics provide information regarding hits, misses, or false alarms, they do not shed any light on the biases and errors in the magnitude of the variable observed (which, in this case, is rainfall in mm/day). Recently, AghaKouchak and Mehran [78] have extended the commonly used categorical metrics to their volumetric equivalents which decompose the total error/bias in terms of their respective volumetric error components. If ORB and $APHRO$ represent the daily rainfall in mm/day from orbital data products and the reference APHRODITE data, respectively, t stands for the threshold (which for example can be rainfall quantile), some of the metrics used for the present study are summarized in Table II. In order to aid in the application of satellite rainfall data, it is essential to understand the error characteristics which are analyzed using various error models and error decomposition techniques, which are briefly explained next.

B. Modeling Errors Using Additive and Multiplicative Models

An error model mathematically defines the deviation of a derived value from the ground truth. Once the parameters of an error model are known, they can be used to further predict

TABLE II
LIST OF PERFORMANCE MEASURES USED FROM CONTINGENCY TABLE

Serial No.	Performance measure	Formula
1.	Probability of Detection (POD)	$\frac{H}{H+M}$
2.	False Alarm Ratio (FAR)	$\frac{F}{H+F}$
3.	Critical Success index (CSI)	$\frac{H}{(H+M+F)}$
4.	Volumetric hit index (VHI)	$\frac{\sum_{i=1}^{n}(ORB_i \mid (ORB_i > t \,\&\, APHRO_i > t))}{\sum_{i=1}^{n}(ORB_i \mid (ORB_i > t \,\&\, APHRO_i > t)) + \sum_{i=1}^{n}(APHRO_i \mid (ORB_i \le t \,\&\, APHRO_i > t))}$
5.	Volumetric False alarm ratio (VFAR)	$\frac{\sum_{i=1}^{n}(ORB_i \mid (ORB_i > t \,\&\, APHRO_i \le t))}{\sum_{i=1}^{n}(ORB_i \mid (ORB_i > t \,\&\, APHRO_i > t)) + \sum_{i=1}^{n}(ORB_i \mid (ORB_i > t \,\&\, APHRO_i \le t))}$
6.	Volumetric miss index (VMI)	$\frac{\sum_{i=1}^{n}(APHRO_i \mid (ORB_i \le t \,\&\, APHRO_i > t))}{\sum_{i=1}^{n}(ORB_i \mid (ORB_i > t \,\&\, APHRO_i > t)) + \sum_{i=1}^{n}(APHRO_i \mid (ORB_i \le t \,\&\, APHRO_i > t))}$
7.	Volumetric Critical Success index (VCSI)	$\frac{\sum_{i=1}^{n}(ORB_i \mid (ORB_i > t \,\&\, APHRO_i > t))}{\sum_{i=1}^{n}((ORB_i \mid (ORB_i > t \,\&\, APHRO_i > t)) + (APHRO_i \mid (ORB_i \le t \,\&\, APHRO_i > t)) + (ORB_i \mid (ORB_i > t \,\&\, APHRO_i \le t)))}$

the parameters and their associated uncertainties when just ground reference data are made available. The availability of different error models often tends to raise confusion among end users regarding their suitability. Some studies considered multiplicative error models [77]–[80], whereas some others depended on additive error models [55], [78]. Motivated by this diversity, this paper discusses both types of error models. The additive error model defines error to be the arithmetical difference between the derived value and ground truth

$$Y = A + BX + \varepsilon \tag{1}$$

where A and B denote the systematic error which is deterministic in nature, ε represents the random component of error, which is assumed to have zero mean and a constant variance of σ^2, Y stands for derived value (TRMM level 2 data in our case) and X represents reference data (APHRODITE data in the present study). The parameters of the additive model can be estimated using ordinary least squares (OLS) approach assuming the random errors (or white noise) to be normally distributed and uncorrelated with a constant variance of σ^2. The multiplicative model is defined as

$$Y = AX^B e^{\varepsilon}. \tag{2}$$

Here, systematic error (i.e., A, B) is assumed to be nonlinearly related to the reference data and random component of error (denote by e^{ε}) which is a multiplicative factor. It is to be noted that the value of A, B and σ will be different for the additive and multiplicative models [81]. The multiplicative error model can be solved using the OLS approach after performing natural logarithmic transformation of the variables.

C. Error Decomposition Into Systematic and Random Components

Previous studies had reported uncertainty of data products by focusing on investigation, quantification and propagation of uncertainty in hydrological model simulation. One of the very first studies in this regard was carried out by Huffman *et al.* [82] who formulated an expression for estimating the root mean square random error in area-time averaged precipitation estimates using the average precipitation rate and the probability distribution parameters of precipitation estimates. The results on uncertainty analysis reported a dominant contribution of algorithmic error over the sampling error. A comprehensive study on algorithmic uncertainty was conducted by Tian and Peters-Lidard [83] who developed a global map of satellite rainfall uncertainty depicting both systematic and random error components. Results revealed relatively smaller uncertainty over oceans, compared with land mass. The systematic and random error components of precipitation retrieval algorithms are known to interact nonlinearly with the uncertainty of hydrologic models thereby further contributing to the uncertainty in the simulation of runoff at the watershed scale or in the resulting flood forecasts [84]–[87]. These studies have not addressed the time-dependent biases that exist within TRMM orbital data products, which may cause significant errors when used for climate related studies. The error in numerical weather prediction models can be segregated into their corresponding systematic and random error components using the Willmott Decomposition technique [88]. For the present study, the total mean squared error (MSE) will be decomposed into its two components: systematic error [MSE_{SYS}, first term in (3)], to which a linear function can be fitted [86] and random error [MSE_{RAN}, second term in (3)]

$$\frac{\left(\sum_{i=1}^{n}(R_{ORB}-R_{APHRO})^2\right)}{n} = \frac{\left(\sum_{i=1}^{n}(R^*_{ORB}-R_{APHRO})^2\right)}{n} + \frac{\left(\sum_{i=1}^{n}(R_{ORB}-R^*_{ORB})^2\right)}{n} \tag{3}$$

where R_{ORB} denotes rainfall estimates from TRMM level 2 data products; R_{APHRO} denotes rainfall from the reference

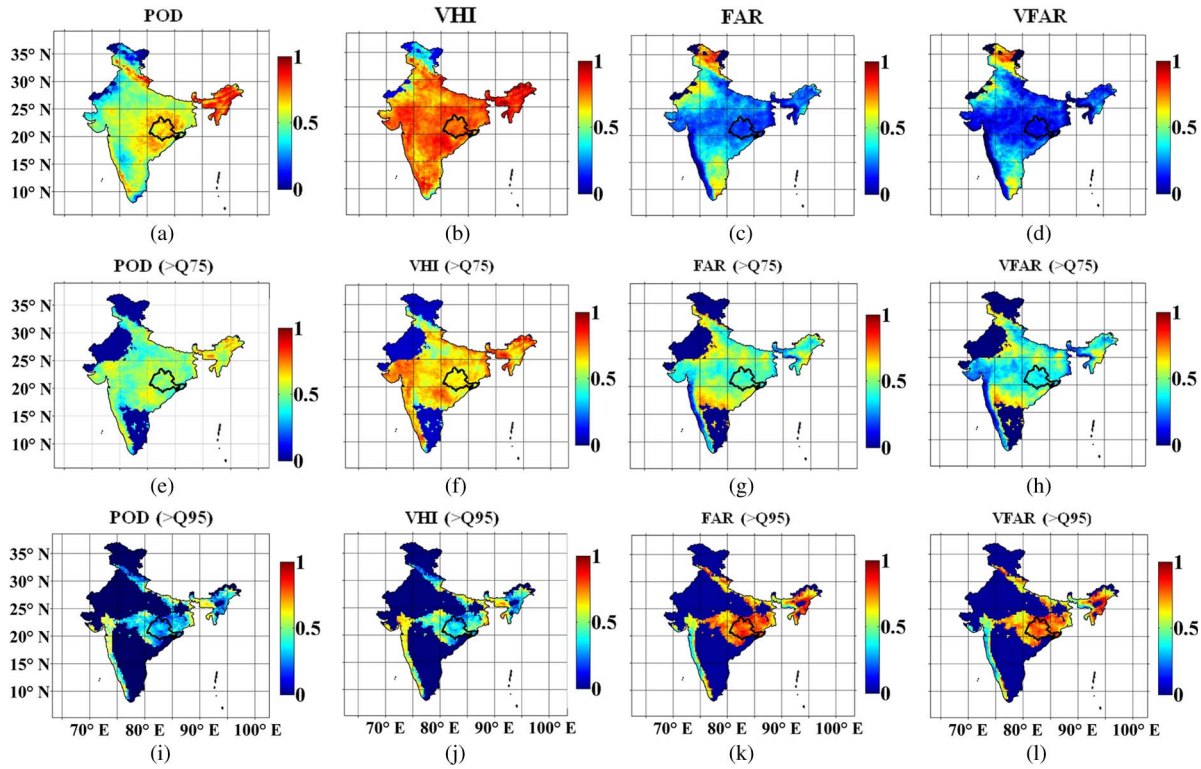

Fig. 1. Spatial distribution of performance metrics over India showing POD, VHI, FAR, and VFAR for a daily time scale, for rainfall estimates $>$ 75th quantile and $>$ 95th quantile.

APHRODITE data product; and R^*_{ORB} denotes $A + B^* R_{APHRO}$ (where A, B denote the intercept and slope, respectively).

V. Results and Discussion

A. Graphical Analysis of Seasonal Precipitation Over India

Prakash *et al.* [90] have analyzed four independently developed multisatellite high-resolution precipitation products, namely, Climate Prediction Center Morphing (CMORPH), Naval Research Laboratory (NRL) blended Precipitation Estimation from Remotely Sensed Information using Artificial Neural Networks (PERSIANN) and TMPA with respect to rain gauge data over India for a 6-year period from 2004 to 2009 at daily scale for the summer monsoon season of June to September. Their study indicated rainfall estimates from TMPA product to be best with a low rate of underestimation and a higher correlation. For the present study, performance of daily precipitation from TMPA is evaluated over the Indian subcontinent with respect to the APHRODITE rainfall (as reference) over a spatial scale of $0.25^\circ \times 0.25^\circ$. The period of study considered is the JJAS months of 2002–2007.

Results of comparative evaluation using the contingency table metrics are presented in Figs. 1 and 2 for daily and higher quantiles of rainfall. It should be noted that the results are being presented for rainfall exceeding 75th and 95th quantiles, which corresponds to 5.5 and 24 mm/day for India. Pertaining to the present study, Probability of Detection (POD) represents the ratio of number of correct identifications of TMPA to the total number of reference (APHRODITE) precipitation occurrences and the volume of hit index (VHI) represents the volume of TMPA precipitation that gets correctly detected. For the seasonal rainfall from Fig. 1(a), one can observe that, POD values lie between 0.3–0.5, whereas VHI values range from 0.7 to 0.9 implying that TMPA detects more than 75% of the volume of observed precipitation (the regions of Jammu Kashmir and northern Rajasthan are significant exceptions). Jiangnan *et al.* [91] has stated that the proportion of stratiform precipitation of the Indian monsoon season attains a maximum value during summer. This implies that for the seasonal rainfall over India, most of the missed events in TMPA are light rainfall events/stratiform rainfall. However, for higher rainfall quantiles (i.e., Q75 and Q95), POD and VHI from Fig. 1 (e), (f), (i), and (j) indicate that as the threshold for heavy rain rate increases, both POD and VHI tends to decrease. Similarly, a comparison between Fig. 1(c) and (d) shows that the false alarm ratio (FAR) values are relatively larger than volumetric FAR (VFAR) values particularly around the north westerns parts of India. Both FAR and VFAR were found to increase at higher thresholds of Q75 and Q95 [see Fig. 1(g)–(l)]. It should be noted that the values of POD, VHI, FAR, and VFAR are near zero at the higher quantiles across much of India because in these regions rain rates corresponding to these quantile values do not occur. From Fig. 1(i) and (j), it can be observed that region of eastern India (location of Mahanadi basin) and south western coastline are subjected to higher volume of rainfall during the Indian summer monsoonal season. Fig. 1(k) and (l) indicates that these regions possess a higher FAR and VFAR values implying poor detection of higher rainfall quantiles by TMPA. The MISS index and volumetric miss index (VMI) from Fig. 2(k) and (l) also suggest that the performance of TMPA is affected over eastern India. The critical success index (CSI) values [see Fig. 2(a)] over majority of Indian regions show that the overall performance score of TMPA over India is between 0.3 and 0.6, whereas the

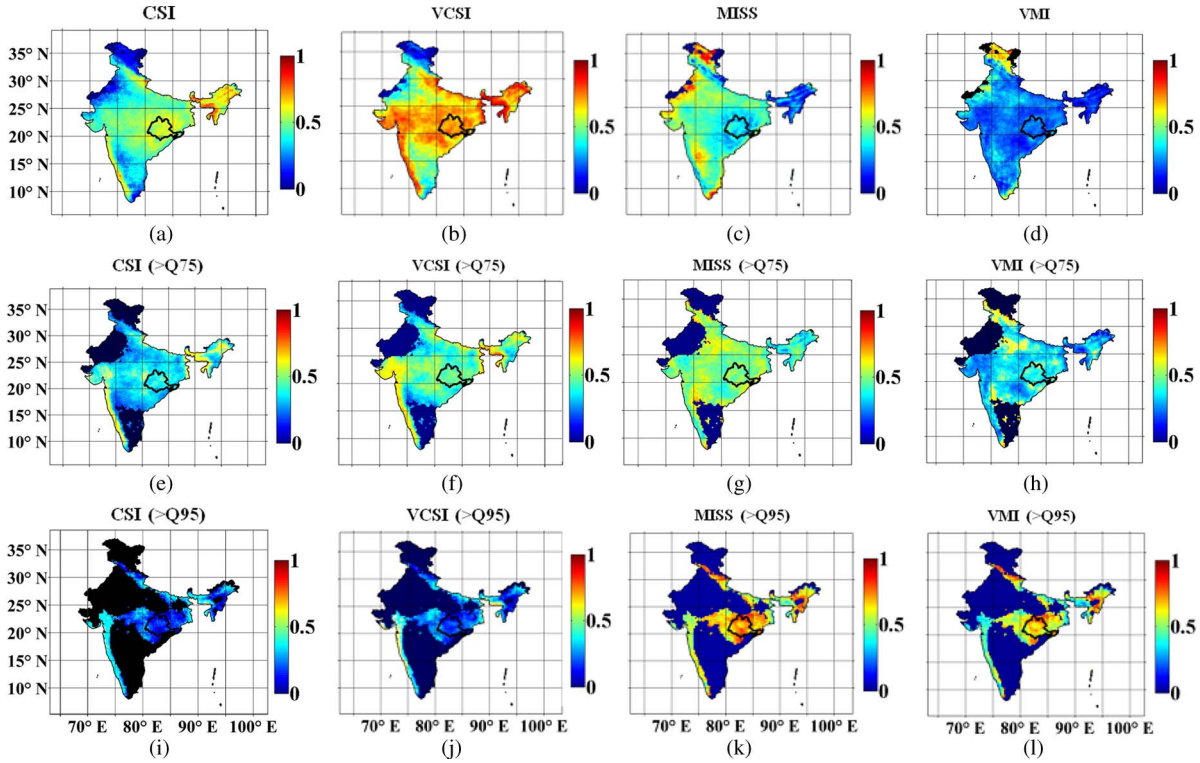

Fig. 2. Spatial distribution of performance metrics over India showing CSI, VCSI, MISS, VMI for a daily time scale, for rainfall estimates > 75th quantile and > 95th quantile.

overall measure of volumetric performance given by volumetric critical success index (VCSI) [see Fig. 2(b)] indicates a higher performance score (between 0.6 and 0.8). From the MISS index [see Fig. 2(c)] one can conclude that TMPA fails to detect a large fraction of precipitation. However, VMI [see Fig. 2(d)] suggests that the volume of precipitation that TMPA does not detect is relatively small.

To summarize, graphical evaluation of TMPA for Q75 and Q95 [see Fig. 2(e)–(l)] shows that as the threshold of detection is increased, the indices of CSI, VCSI, MISS, and VMI lose their skill over India particularly over parts of southwestern coastline and over Mahanadi basin indicating that TMPA data product fails to detect rainfall extremes (above Q75 and Q95). To support the choice of the study region, the results presented over India for overall rainfall, rainfall > 75th and > 95th quantiles indicate that, in particular, the Eastern part of India is subjected to poor detection of higher quantiles of rainfall.

Among these regions, the basin of Mahanadi (see Fig. 3), situated between latitudes 19° N to 24° N and longitudes 80° E to 87° E, is relevant from a hydrologic perspective owing to the fact that it receives heavy to very heavy rainfall during Indian Summer Monsoonal Season (when monsoon depressions from the Bay of Bengal move north-westward slightly south of their normal track). The basin has been repetitively facing adverse hydrometeorological conditions such as floods, droughts, and cyclones in recent times. The orography of the Eastern Ghats also influences the rainfall pattern over the basin to a great extent.

One of the major applications of TRMM rainfall retrieval products is to assist in real time flood forecasting and rainfall–runoff studies. Although there are several sources of uncertainty

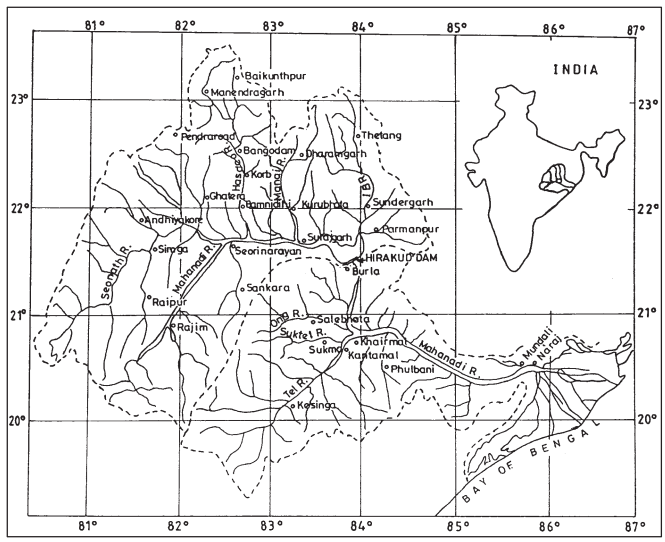

Fig. 3. Geographical location of Mahanadi basin, India.

that complicate our understanding of flood prediction accuracy, the principal source of uncertainty is, undoubtedly, rainfall [91], [92]. When remotely sensed data products are used as an input to the hydrological models, the error characteristics of these rainfall products propagate in the resulting prediction of hydrologic parameters. Meaningful applications of microwave rainfall estimates often require a proper understanding of the underlying errors contributed by these products. Keeping this in mind, for the present study, the performance of TRMM products are investigated over the basin of Mahanadi, India.

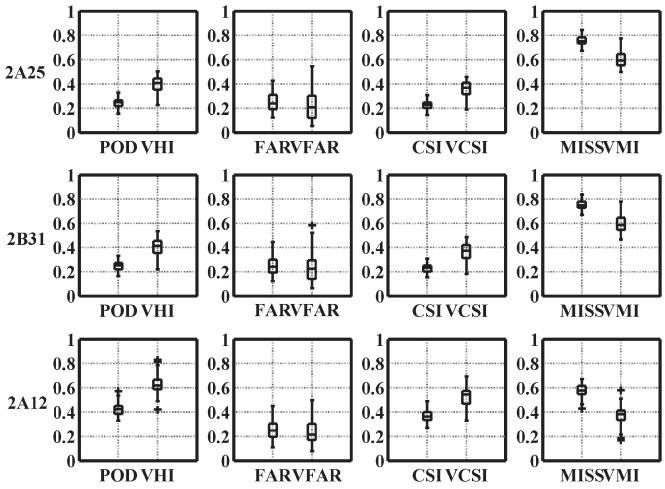

Fig. 4. Box plots showing POD, VHI, FAR, VFAR, CSI, VCSI, MISS, and VMI for daily rainfall estimates over Mahanadi basin obtained using 2A25, 2B31, and 2A12 data.

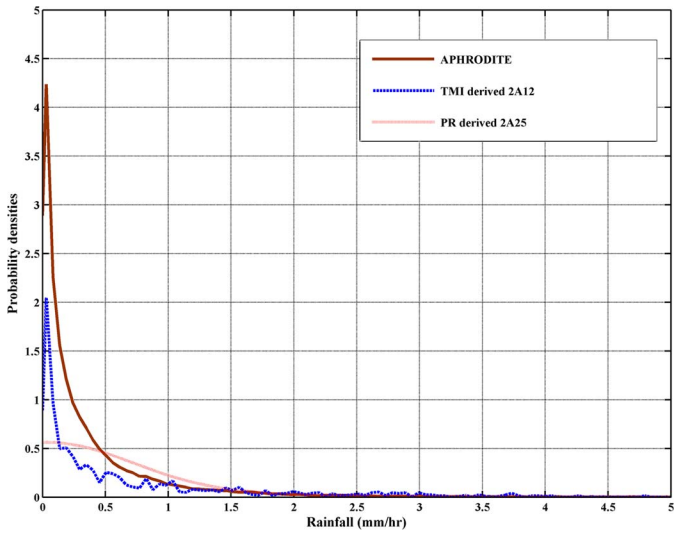

Fig. 5. Pdf showing seasonal rainfall in mm/hr from APHRODITE, 2A12, and 2A25 for 1° × 1° grid boxes over Mahanadi basin from June 2002 to September 2007.

B. Seasonal Precipitation Over Mahanadi Basin

This section investigates the uncertainty contributed by three of the TRMM level 2 data products over Mahanadi basin. If an event that any portion of the TRMM orbital swath covers within the 1° spatial grid box is termed as a visit, then, the TRMM orbital data provides the number of pixels N and the mean rainfall rate R (mm/hr) over the grid box at each visit. If n is the number of times during which TMI/PR observes rainfall in a spatial scale/grid box for any time period, then the average rainfall amount within any space time domain can be estimated using the relation

$$R_S = \frac{\sum_{i=1}^{n} N(i)^* R(i)}{\sum_{i=1}^{n} N(i)}. \tag{4}$$

For the present study, rainfall estimates (in mm/hr) from multiple TRMM overpasses of a single day are averaged giving equal weight to all the values to create the daily rainfall values over each space scale (grid boxes) over Mahanadi basin for the JJAS months from 2002–2007. The total number of orbital data points during the 6-year period that were considered for the creation of daily gridded rainfall estimates are 2548 for 2A25 data, 3535 for 2B31 data, and 3552 for 2A12 data set, respectively, which corresponds to 3.48 scenes per day 2A25, 4.83 for 2B31, and 4.85 for 2A12. It is to be noted that selection of an appropriate grid size for the orbital products warrants a compromise between two major competing factors. First, the grid size chosen should be as large as possible, which enables one to treat rainfall averages over each grid box as statistically independent thereby allowing the use of statistical measures for further analysis. Second, a realistic representation of local rainfall rate with minimum error requires the grid size chosen to be as small as possible, which allows rainfall rates within each grid to be approximately homogeneous. A previous sampling error related study over the basin using PR 2A25 data product yielded 1° × 1° as a suitable space scale for analysis owing to comparatively lower relative sampling errors [93]. Keeping these factors in mind, a grid size of 1° × 1° was chosen for the present study.

The various performance measures for daily rainfall estimates using 2A25, 2A12, and 2B31 data over the case study region of the Mahanadi basin are shown in Fig. 4. It can be observed that the value of POD is highest for 2A12 (value between 0.4–0.6), whereas POD values for 2B31 (value < 0.3) and for 2A25 (value < 0.3) are comparatively lower. This has interesting implications in the volumetric context as pointed out in [78]. The volume of precipitation obtained by VHI for all three products for daily seasonal rainfall show that a high VHI does not necessarily lead to a high POD when a small percentage of detected occurrences constitute a large volume of the total rainfall, as is evident for 2B31 and 2A25. However, the FAR and VFAR values are similar to each other for all three data products. The observed values for CSI for daily precipitation are found to be relatively higher for 2A12 (0.4–0.6) than those observed for 2A25 and 2B3 (< 0.4). Comparisons of missed precipitation and VMI show that rainfalls from 2A12 data product are in better agreement with the reference estimates, as compared with 2A25 and 2B31 data products.

Fig. 4 shows that the 2A25 and 2B31 data products tend to behave in a more or less similar manner. For rainfall estimations over land, the 2B31 data product uses the ice scattering signal at relatively high frequencies [90], [93], [94] and relies entirely on the radar inversion technique to estimate rainfall [47]. The 2B31 data product works as a combined radar-radiometer product only over the oceans and serves as mostly a radar only product over the land [46]. This is because for rainfall retrievals over the land regions, the active radar is more accurate than the passive radiometer. Hence, the active radar is heavily relied upon for retrievals over land, thereby making 2B31 very similar to 2A25 over the land regions. Hence, further discussions are limited to comparative evaluation between the 2A12 and 2A25 data products.

Results indicate that for the seasonal daily precipitation over 1° × 1° grids, 2A12 showed greater skill in detecting and quantifying the volume of rainfall when compared with the 2A25 data products. Studies by Indu and Kumar [97] have showed that over the basin, vertical distribution of hydrometeors will be dominated by bottom heavy liquid water indicating stratiform rainfall type. The PR detects rainfall at a threshold

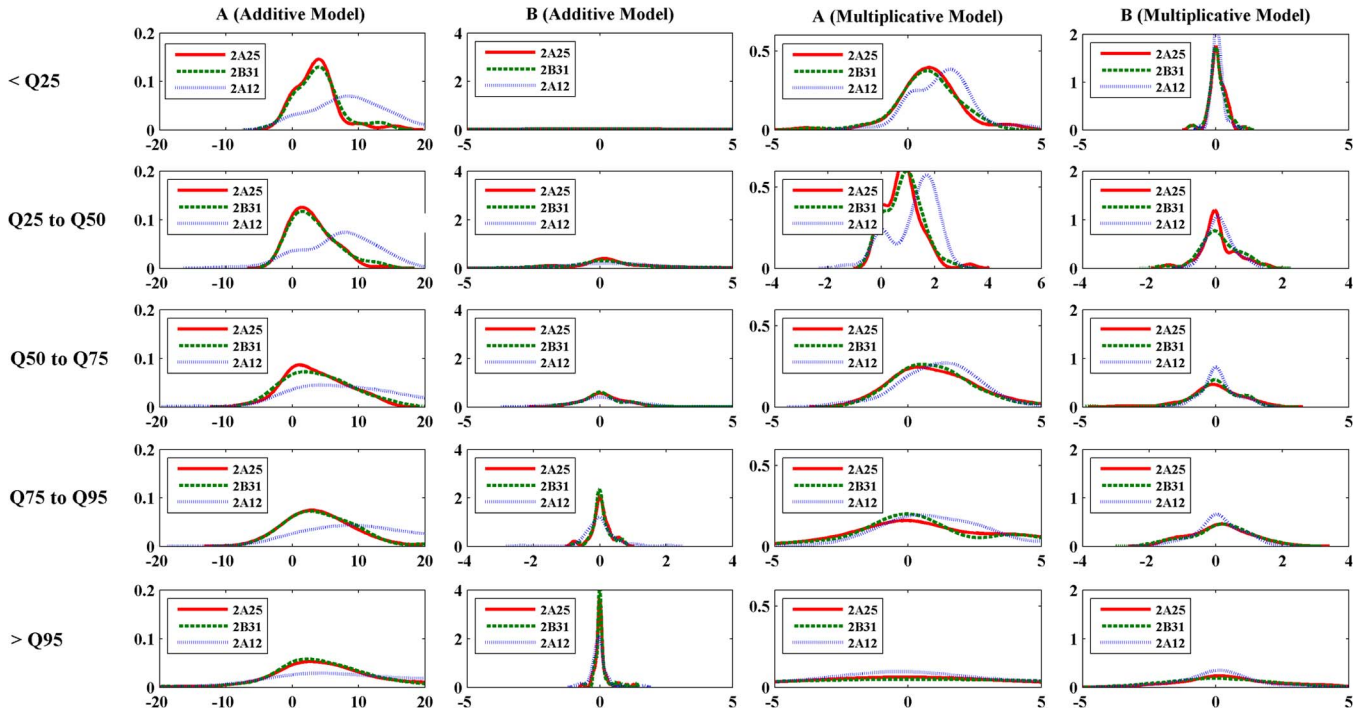

Fig. 6. Distribution of model coefficients of the additive and multiplicative error models estimated for each quantile class of rainfall for 2A25, 2A12, and 2B31 rainfall estimates.

of ∼18 bBZ, which makes it very difficult to detect rainfall below 0.4 mm/hr. Although the TMI derived 2A12 is capable of detecting precipitation of 0.1 mm/hr, it is unable to detect warm rainfall over land [39]. Both these products are susceptible to poor detection at the lightest rain rates. Furthermore, studies by Kirstetter *et al.* [98] have addressed the case of PR detecting no rainfall during rainfall conditions thereby highlighting the poor detection by PR toward light rain rates [95]. This can also be observed from Fig. 5, which shows the pdf of seasonal rainfall from APHRODITE, 2A12, and 2A25 over Mahanadi basin. The pdf indicates that, in spite of the difficulty in detecting light rainfall, over the basin, rain rates > 1 mm/hr are successfully detected by TMI thereby demonstrating superior performance by 2A12 algorithm.

Despite the tendency of the radiometer retrieved 2A12 land rainfall algorithm to overestimate rainfall during deep convective processes, their land rainfall is found to be in remarkable agreement with the reference observations for the data period considered. The better performance of 2A12 land rainfall algorithm in comparison with 2A25 algorithm over the basin can be attributed to its database consisting of preexisting rainfall profiles carefully selected so that the resulting rainfall retrieved by scattering scheme is consistent with ground-radar measurements. This is because the 2A12 algorithm based on cloud-resolving models that focus mainly on the tropical precipitation thereby explaining its better performance over the study region.

However, there exist time-dependent regional biases, which exist between TRMM orbital data products that impact the appropriateness of the data for regional climate studies or investigation of climate variability. This is because satellite rainfall retrieval algorithms depend on a number of parameter assumptions, which are not directly measured by the satellite. Owing to the variations in the value of these parameters across various meteorological regimes, regional/temporal biases occur in the resulting rainfall estimates. Biases shown by algorithms of 2A12 and 2A25 vary with changes in cloud microphysics during precipitating system life cycles [22]. When the rainfall estimates are averaged over large space and time scales, usually the random errors diminish leaving the systematic errors, which can significantly affect climate applications.

One of the major challenges in hydrological applications is to characterize this systematic error on a daily time scale for the JJAS months. Adequate considerations should be given to the uncertainties in these data sets prior to utilizing them in hydrologic and climatic studies. If it is assumed that the reference data (APHRODITE) represents the most probable value of true rainfall occurring over a spatial domain (of $1^\circ \times 1^\circ$ grid size) over Mahanadi basin, the residuals between the estimated rainfall (from 2A12, 2A25, and 2B31) and reference values can be used to build error models for characterizing the uncertainty.

C. Error Model Analysis

The present study classified daily rainfall intensities falling in each spatial domain ($1^\circ \times 1^\circ$ grid box) over Mahanadi basin into 5 different quantile classes: i) < 25th ; ii) 25th–50th; (iii) 50th–75th; (iv) 75th–95th; and (v) $>$ 95th. Based on these 5 different classes, for each spatial grid over Mahanadi basin, the coefficients of additive and multiplicative error models were estimated independently. The analysis was performed independently for the 2A12, 2A25, and 2B31 data products. Fig. 6 shows the distribution of model coefficients obtained over Mahanadi basin. The plot shows the distribution of coefficients A and B for both additive and multiplicative error models, which define the deterministic error component. For additive error model, there is large variation in the coefficient A for 2A12 particularly for low intensity rainfall. Visual examination shows a near Gaussian pattern of coefficients B for both additive and

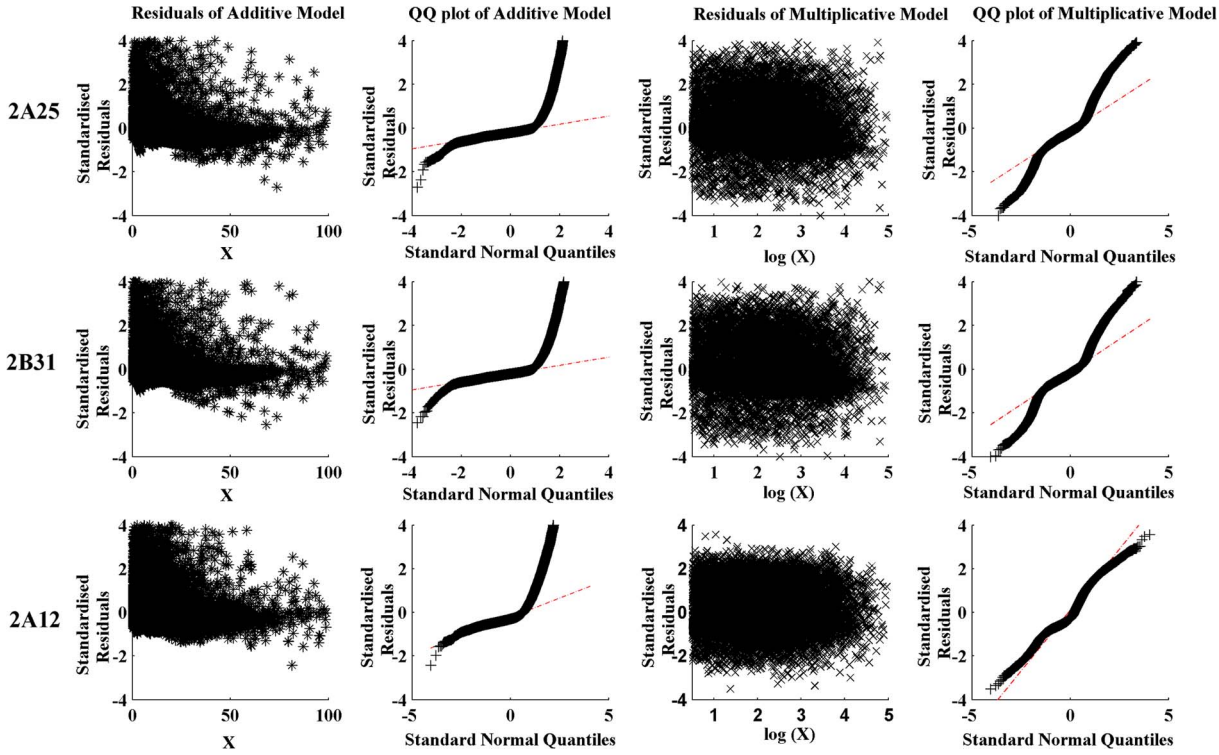

Fig. 7. Standardized residual plots and quantile–quantile plots of 2A25, 2A12 and 2B31 for (a) additive error model and (b) multiplicative error model. The dotted line in the plot joins the first and third quartiles of each distribution and is extrapolated to the ends to help evaluate the linearity of the data.

multiplicative error models. The distribution of model coefficients is useful when each of these models is utilized to model the large dynamical range of precipitation data. This will be taken up as part of a future study pertaining to Mahanadi basin.

Using the model coefficients for each quantile class of rainfall, both models were fitted for the Mahanadi basin and their respective standardized residual plots were obtained (i.e., residuals of each model normalized by their respective standard deviation as shown in Fig. 7). Fig. 7 shows that the two error models behave quite differently. The standardized residual plots for the additive model exhibit a systematic increase in scattering with higher rain rates, whereas the residuals for the multiplicative model show a fairly constant range of variation. This implies that random errors produced by additive model are not homoscedastic (having a constant variance). These findings reveal the violation of constant variance assumption made in the estimation of model parameters using OLS regression approach. Furthermore, they also imply that the additive model fails to remove some systematic errors, which get leaked into the random errors thereby inflating the uncertainty. Studies by Tian *et al.* [81] have stated that such a leak occurs due to the linearity assumption between systematic errors and reference data. However, studies by Gebremichael *et al.* [10] have also indicated otherwise. The quantile–quantile plots for standardized residuals show that fitting using additive error model results in standardized residuals that violate the assumption of being normally distributed for all three data products.

However, the multiplicative error model was found to fit the whole range of the data in a much better manner. Compared with the additive model for 2A25 and 2A12 algorithm, the multiplicative model for 2A12 data showed a better fit. A similar conclusion can be made regarding the normal quantile plot of standardized residuals (see Fig. 7). For the additive model, Fig. 7 shows a reasonably linear pattern in the center of the data for both 2A25 and 2A12. However, a large departure can be observed along the tails at each end of the distribution for both these data products. This implies that the additive model failed in analyzing higher and lower estimates of rainfall. On the contrary, for the multiplicative error model, Fig. 7 shows that results obtained from 2A12 algorithm depict a much better agreement along the line, as compared with 2A25 algorithm.

It is worthwhile to note that log transformation within a multiplicative error model places variable values into a geometric domain wherein proportional deviations get represented independently of the scale/units of measurement. Results indicate that for the rainfall from TRMM level 2 data products, as the underlying phenomena are fundamentally multiplicative, their rainfall estimates are more likely to conform to a multiplicative error model [100], [101]. It can be concluded that, assuming additive variation of errors as the default standard for TRMM level 2 rainfall estimates, can prove erroneous particularly when examining patterns across many orders of magnitude, because the same relative deviation will be a much smaller absolute (arithmetic) deviation for small observations than for large observations. In order to examine the relative suitability of the two models, the total error needs to be decomposed into its systematic and random parts.

D. Systematic and Random Error

For the present study, an error decomposition technique based on the Willmott Decomposition technique was used to arrive at the systematic and random error components as

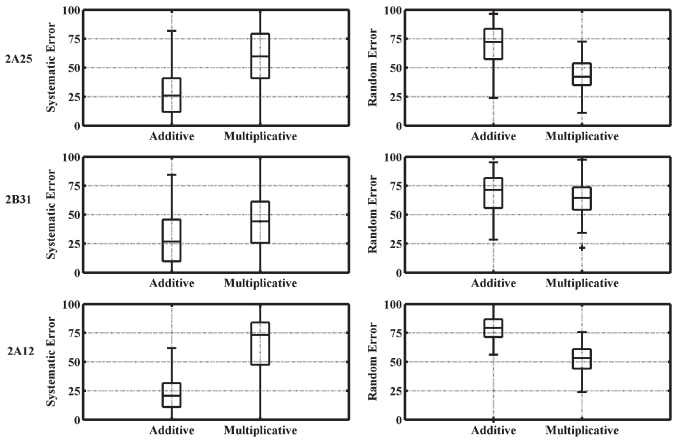

Fig. 8. Spatial distribution of systematic and random error (in %) of 2A25, 2A12, and 2B31 for the additive and multiplicative error models.

explained in Section IV-C. Ideally, the systematic error is the component which is to be minimized or is to be removed. With several sources of errors in the grid averaging, it is important to quantify how much of the deviation between TRMM level 2 products and the reference data can be attributed to random versus systematic causes.

The error decomposition method is applied individually using additive and multiplicative error models for each of the three TRMM algorithms and the results are displayed in Fig. 8. If MSE_{TOT} represents the total mean squared error and MSE_{SYS} and MSE_{RAN} depict the systematic and random components of mean squared error, the systematic error is represented as $MSE_{SYS}/MSE_{TOT} \times 100$ and random error is estimated as $MSE_{RAN}/MSE_{TOT} \times 100$, which are the components of the total MSE (in %) for daily precipitation data for the monsoonal season over the case study region. A better error model should ideally capture more signal from the noise. In other words, as systematic error refers to the part, which can be deterministically described, majority of the total deviation within an error model needs to be attributed to the deterministic component of uncertainty (systematic error) thereby leaving a minimum amount of unexplainable deviation to be explained by random error. A comparative evaluation of the systematic and random errors explained by the additive error model reveals that both 2A25 and 2A12 data products exhibited systematic errors up to 75% (for 2A25) and 60% (for 2A12). Comparatively, the systematic errors explained by the multiplicative error model ranged up to nearly 100% for both 2A25 and 2A12 data products. The systematic errors of multiplicative error model was found to be nearly normal for 2A25 (with median of box plot at nearly 60%) and skewed for 2A12 (with median toward upper quantile at nearly 75%). Overall, a greater percentage of systematic errors were explained by the multiplicative error model for 2A12 than 2A25 data. The multiplicative error model depicted a more compact range of random errors for 2A12 data (ranging from 25–75%) when compared with a wider ranger for 2A25 data (range between 10–75%). The multiplicative error model is a better choice for explaining the inconsistencies in the wide range of precipitation variability offered by 2A12 data product. Hence, this model can be used for uncertainty quantification of daily precipitation estimates from TRMM orbital data products.

VI. Conclusion

The TRMM products development team provides various precipitation products either based on radar (PR) or radiometer (TMI) or a combination of both (PR-TMI). This study analyzed the spatial error characteristics of daily rainfall from the latest v7 precipitation estimates of TMI and PR products namely the 2A12, 2A25, and 2B31 data. Results are presented over the basin of Mahanadi using six years of monsoon data period from June 2002 to September 2007. The total numbers of orbital data points from the 6-year period considered for the creation of gridded data set are 2548 for 2A25 data, 3535 for 2B31 data and 3552 for 2A12 data set. A space scale of $1^\circ \times 1^\circ$ was deemed suitable for gridding the rainfall estimates from each individual snapshot of orbital data. The findings of this study are summarized as follows:

1) Spatial variation of various performance measures were analyzed for the 2A25, 2A12, and 2B31 data products using indices derived from the contingency table. Higher values for POD were obtained for 2A12 (value between 0.4–0.6) compared with the POD values for 2B31 (value < 0.3) and for 2A25 (value < 0.3). The volumetric indices from the contingency table [75] were utilized to decompose the total volumetric error into volumetric hit index, VFAR, VMI, and volumetric critical success index. Despite the limitations in the 2A12 land rainfall algorithm, their daily rainfall estimates over the Mahanadi basin for the JJAS summer monsoonal months showed a better agreement with the APHRODITE reference data than the 2A25 rainfall.

2) As the 2A12 product (from radiometer TMI) and 2A25 (from radar PR) were generated based on different sensors, the plausible reasons for the uncertainty in rainfall detection was attributed to the properties of these sensors along with the properties of seasonal rainfall occurring over the basin. Uncertainty of PR 2A25 algorithm was attributed to the low sampling by PR as compared with TMI, which implies comparatively lower number of observations during different times of the day for PR over Mahanadi basin. The underestimation by the PR 2A25 algorithm was explained to be due to the strong attenuation of radar reflectivity by atmospheric ice and its poor sensitivity toward stratiform rainfall. Although the TMI 2A12 algorithm has limited ability to detect warm rainfall over land, their daily rainfall estimates were found to agree well with the reference rainfall.

3) The residual errors between rainfall estimates of gridded orbital data products and reference rainfall estimates were utilized to create additive and multiplicative error models. The parameters of these models were estimated for each $1^\circ \times 1^\circ$ grid box over the basin by dividing rainfall intensities into 5 different quantile classes, namely: i) < 25th; ii) 25th–50th; iii) 50th–75th; iv) 75th–95th; and v) > 95th. Results based on standardized residual plot revealed that the residuals of the multiplicative error model were homoscedastic compared with the additive error model. The multiplicative error model was found to better depict rainfall estimates based on the 2A12 data product. This questions the assumption of additive variation of errors as the default standard in analyzing rainfall estimates.

4) The total MSE was decomposed into its systematic and random error components using Willmott decomposition

technique. Results show that for the multiplicative error model, rainfall estimates from the 2A12 algorithm exhibited larger systematic errors compared with the 2A25 algorithm. In other words, for 2A12, the majority of the total deviation was attributed to the deterministic component of uncertainty. The present study is conducted over a single subtropical basin over Indian region. This approach can however be potentially extended to other tropical regions of the world by comparing with the regional meteorological data products.

To summarize, the uncertainty in rainfall retrieval by PR-derived rainfall products is dominated mainly due to sampling issues and partly owing to the PR's insensitivity to light rainfall (< 0.7 mm/day), uncertainty related with *a priori* selection of DSD, nonuniform beam filling effects, incorrect physical assumptions of freezing level height, hydrometeor temperature, etc. [4].

Although rainfall estimates from the PR-based 2A25 algorithm are known to perform well over land, regional biases influence the performance for daily time scales as is evident from the present study. Improving the accuracy and error characterization of TRMM level 2 rainfall estimates is critical for a number of satellite rainfall products and applications because the uncertainties tend to propagate to TRMM based multisatellite rainfall estimates. The current mission of GPM envisions a constellation of passive microwave sensors that will provide products with a relatively negligible sampling error at daily or higher time scales. This study by means of its simplicity and physical approach is aimed toward future improvements in uncertainty modeling of precipitation.

ACKNOWLEDGMENT

The authors would like to thank the Goddard Distributed Active Archive Center for providing the TRMM science data products. The first author would like to thank Dr. A. AghaKouchak (University of California, Irvine) and Dr. Y. Tian (NASA Goddard Space Flight Center) for providing valuable and insightful suggestions enabling this study to materialize.

REFERENCES

[1] G. W. Petty, "Physical retrievals of over-ocean rain rate from multichannel microwave imaging. Part I: Theoretical characteristics of normalized polarization and scattering in-dices," *Meteorol. Atmos. Phys.*, vol. 54, no. 1–4, pp. 79–99, 1994

[2] G. W. Petty, "Physical retrievals of over-ocean rain rate from multichannel microwave imaging. Part II: Algorithm implementation," *Meteorol. Atmos. Phys.*, vol. 54, no. 1–4, pp. 101–122, 1994.

[3] T. T. Wilheit and A. Al Khalaf, "A simplified interpretation of the radiances from the SSM/T-2," *Meteorol. Atmos. Phys.*, vol. 54, no. 1–4, pp. 203–212, 1994.

[4] C. Kummerow, W. S. Olson, and L. Giglio, "A simplified scheme for obtaining precipitation and vertical hydrometeor profiles from passive microwave sensors," *IEEE Trans. Geosci. Remote Sens.*, vol. 34, no. 5, pp. 1213–1232, Sep. 1996.

[5] W. S. Olson, C. D. Kummerow, G. M. Heymsfield, and L. Giglio, "A method for combined passive-active microwave retrievals of cloud and precipitation profiles," *J. Appl. Meteorol.*, vol. 35, no. 10, pp. 1763–1789, Oct. 1996.

[6] R. R. Ferraro, "Special sensor microwave imager derived global rainfall estimates for climatological applications," *J. Geophys. Res.*, vol. 102, no. D14, pp. 16 715–16 735, Jul. 1997.

[7] R. R. Ferraro *et al.*, "NOAA operational hydrological products derived from the Advanced Microwave Sounding Unit," *IEEE Trans. Geosci.Remote Sens.*, vol. 43, no. 5, pp. 1036–1049, May 2005.

[8] E. A. Smith *et al.*, "Results of WetNet PIP-2 project," *J. Atmos. Sci.*, vol. 55, no. 9, pp. 1483–1536, May 1998.

[9] F. Hossain and E. N. Anagnostou, "A two-dimensional satellite rainfall error model," *IEEE Trans. Geosci. Remote Sens.*, vol. 44, no. 6, pp. 1511–1522, Jun. 2006.

[10] M. Gebremichael, G.-Y. Liao, and J. Yan, "Nonparametric error model for a high resolution satellite rainfall product," *Water Resour. Res.*, vol. 47, no. 7, Jul. 2011, Art. ID. W07504.

[11] F. Hossain and G. Huffman, "Investigating error metrics for satellite rainfall data at hydrologically relevant scales," *J. Hydrometeorol.*, vol. 9, no. 3, pp. 563–575, Jun. 2008.

[12] M. Pan, H. Li, and E. Wood, "Assessing the skill of satellite-based precipitation estimates in hydrologic application," *Water Resour. Res.*, vol. 46, no. 9, Sep. 2010, Art. ID. W09535.

[13] G. J. Huffman *et al.*, "The TRMM multisatellite precipitation analysis (TMPA): Quasi-global, multi-year, combined-sensor precipitation estimates at fine scales," *J. Hydrometeorol.*, vol. 8, no. 1, pp. 38–55, Feb. 2007.

[14] Y. Hong, K. L. Hsu, H. Moradkhani, and S. Sorooshian, "Uncertainty quantification of satellite precipitation estimation and Monte Carlo assessment of the error propagation into hydrologic response," *Water Resour. Res.*, vol. 42, no. 8, Aug. 2006, Art. ID. W08421.

[15] G. Artan *et al.*, "Adequacy of satellite derived rainfall data for streamflow modeling," *Nat. Hazards*. vol. 43, no. 2, pp. 167–185, Nov. 2007.

[16] M. S. Shrestha, G. A. Artan, S. R. Bajracharya, and R. R. Sharma, "Using satellite-based rainfall estimates for streamflow modeling: Bagmati Basin," *J. Flood Risk Manag.*, vol. 1, no. 2, pp. 89–99, Aug. 2008.

[17] F. Su, Y. Hong, and D. P. Lettenmaier, "Evaluation of TRMM multisatellite precipitation analysis (TMPA) and its utility in hydrologic prediction in the La Plata Basin," *J. Hydrometeorol.*, vol. 9, no. 4, pp. 622–640, Aug. 2008.

[18] F. Su, H. Gao, G. J. Huffman, and D. P. Lettenmaier, "Potential utility of the real-time TMPA-RT precipitation estimates in streamflow prediction," *J. Hydrometeorol.*, vol. 12, no. 3, pp. 444–455, Jun. 2011.

[19] H. Wu, R. F. Adler, Y. Hong, Y. Tian, and F. Policelli, "Evaluation of global flood detection using satellite-based rainfall and a hydrologic model," *J. Hydrometeorol.*, vol. 13, no. 4, pp. 1268–1284, Aug. 2012.

[20] R. F. Adler, G. J. Huffman, D. T. Bolvin, S. Curtis, and E. J. Nelkin, "Tropical rainfall distribution determined using TRMM Combined with other satellite and rain gauge information," *J. Appl. Meteorol.*, vol. 39, no. 12, pp. 2007–2023, Dec. 2000.

[21] T. Inoue and K. Aonashi, "A comparison of cloud and rainfall information from instantaneous visible and infrared scanner and precipitation radar observations over a frontal zone in east Asia during June 1998," *J. Appl. Meteorol.*, vol. 39, no. 12, pp. 2292–2301, Dec. 2000.

[22] S. W. Nesbitt, E. J. Zipser, and D. J. Cecil, "A census of precipitation features in the tropics using TRMM: Radar, ice scattering, and lightning observations," *J. Clim.*, vol. 13, no. 23, pp. 4087–4106, Dec. 2000.

[23] D. B. Shin and G. R. North, "Errors incurred in sampling a cyclostationary field," *J. Atmos. Ocean. Technol.*, vol. 17, no. 5, pp. 656–664, May 2000.

[24] T. Wilheit, *Error Analysis for the Tropical Rainfall Measuring Mission (TRMM) in Tropical Rainfall Measurements*. Hampton, VA, USA: A. Depak Publishing, 1988, pp. 377–385.

[25] C. Kummerow, W. S. Olson, and L. Giglio, "The evolution of the Goddard profiling algorithm (GPROF) for rainfall estimation from passive microwave sensors," *J. Appl. Meteorol.*, vol. 40, no. 11, pp. 1801–1820, Nov. 2001.

[26] H. Masunaga, T. Iguchi, R. Oki, and M. Kachi, "Comparison of rainfall products derived from TRMM microwave imager and precipitation radar," *J. Appl. Meteorol.*, vol. 41, no. 8, pp. 849–862, Aug. 2002.

[27] S. W. Nesbitt, E. J. Zipser, and C. D. Kummerow, "An examination of version 5 rainfall estimates from the TRMM microwave imager, precipitation radar, and rain gauges on global, regional and storm scales," *J. Appl. Meteorol.*, vol. 43, no. 7, pp. 1016–1036, Jul. 2004.

[28] V. L. Sanderson, C. Kidd, and G. R. McGregor, "A comparison of TRMM microwave techniques for detecting the diurnal rainfall cycle," *J. Hydrometeorol.*, vol. 7, no. 4, pp. 687–704, Aug. 2006.

[29] D. B. Wolff and B. L. Fisher, "Comparisons of instantaneous TRMM ground validation and satellite rain-rate estimates at different spatial scales," *J. Appl. Meteorol. Clim.*, vol. 47, no. 8, pp. 2215–2237, Aug. 2008.

[30] E. Amitai, X. Llort, and T. D. Sempere, "Comparison of TRMM radar rainfall estimates with NOAA next-generation QPE," *J. Meteorol. Soc. Jpn.*, vol. 87A, pp. 109–118, 2009.

[31] A. P. Barros, G. Kim, E. Williams, and W. Nesbitt, "Probing orographic controls in the Himalayas during the monsoon using satellite imagery," *Nat. Hazards Earth Syst. Sci.*, vol. 4, no. 1, pp. 29–51, Mar. 2004.
[32] A. M. Anders *et al.*, "Spatial patterns of precipitation and topography in the Himalaya," in *Techtonics, Climate and Landscape Evolution*, vol. 398, S. D. Willett, N. Hovius, M. T. Brandon, and D. M. Fisher, Eds., Geological Society of America Special Paper. Boulder, CO, USA: Geological Society of America, 2006, pp. 39–53.
[33] C. Kidd and G. R. McGregor, "Observation and characterization of rainfall over Hawaii and surrounding region from the Tropical Rainfall Measuring Mission," *Int. J. Climatol.*, vol. 27, no. 4, pp. 541–553, Mar. 2007.
[34] K. P. Bowman, A. B. Phillips, and G. R. North, "Comparison of TRMM rainfall retrievals with rain gauge data from the TAO/TRITON buoy array," *Geophys. Res. Lett.*, vol. 30, no. 14, p. 1757, Jul. 2003.
[35] D. B. Shin, J.-H. Kim, and H.-J. Park, "Agreement between monthly precipitation estimates from TRMM satellite, NCEP reanalysis, and merged gauge-satellite analysis," *J. Geophys. Res.*, vol. 116, no. D16, Aug. 2011, Art. ID. D16105.
[36] K. Kikuchi and B. Wang, "Diurnal precipitation regimes in the global tropics," *J. Clim.*, vol. 21, no. 11, pp. 2680–2696, Jun. 2008.
[37] N. Y. Wang, C. Liu, R. Ferraro, E. Zipser, and C. Kummerow, "TRMM 2A12 land precipitation product status and future plans," *J. Meteorol. Soc. Jpn.*, vol. 87A, pp. 237–253, 2009.
[38] K. Gopalan, N.-Y. Wang, R. Ferraro, and C. Liu, "Status of the TRMM 2A12 land precipitation algorithm," *J. Atmos. Ocean. Technol.*, vol. 27, no. 8, pp. 1343–1354, Aug. 2010.
[39] J. P. Zagrodnik and H. Jiang, "Investigation of PR and TMI version 6 and version 7 rainfall algorithms in landfalling tropical cyclones relative to the NEXRAD stage-IV multisensor precipitation estimate dataset," *J. Appl. Meteorol. Climatol.*, vol. 52, no. 12, pp. 2809–2827, Dec. 2013.
[40] A. Y. Hou *et al.*, "The global precipitation measurement mission," *Bull. Amer. Meteorol. Soc.*, vol. 95, no. 5, pp. 701–722, May 2014.
[41] T. Iguchi and R. Meneghini, "Intercomparison of single-frequency methods for retrieving a vertical rain profile from airborne or spaceborne radar data," *J. Atmos. Ocean. Technol.*, vol. 11, no. 6, pp. 1507–1511, Dec. 1994.
[42] T. Iguchi, T. Kozu, R. Meneghini, J. Awaka, and K. Okamoto, "Rain-profiling algorithm for the TRMM precipitation radar," *J. Appl. Meteorol.*, vol. 39, no. 12, pp. 2038–2052, Dec. 2000.
[43] K. Okamoto, R. Meneghini, T. Iguchi, J. Awaka, and S. Shimizu, "TRMM PR algorithms version 6 status and plans for version 7," in *Proc. SPIE, Remote Sens. Atmos. Clouds II*, 2008, vol. 7152, p. 715208.
[44] T. Iguchi *et al.*, "Uncertainties in the rain profiling algorithm for the TRMM precipitation radar," *J. Meteorol. Soc. Jpn.*, vol. 87A, pp. 1–30, 2009.
[45] C. Kummerow, W. Barnes, T. Kozu, J. Shiue, and J. Simpson, "The tropical rainfall measuring mission (TRMM) sensor package," *J. Atmos. Ocean. Technol.*, vol. 15, no. 3, pp. 809–817, Jun. 1998.
[46] Z. S. Haddad *et al.*, "The TRMM 'day-1' radar/radiometer combined rain-profiling algorithm," *J. Meteorol. Soc. Jpn.*, vol. 75, pp. 799–809, 1997.
[47] E. A. Smith, F. J. Turk, M. R. Farrar, A. Mugnai, and X. Xiang, "Estimating 13.8 GHz path-integrated attenuation from 10.7 GHz brightness temperatures for TRMM combined PR- TMI precipitation algorithm," *J. Appl. Meteorol.*, vol. 36, no. 4, pp. 365–388, Apr. 1997.
[48] R. Meneghini *et al.*, "Use of the surface reference technique for path attenuation estimates from the TRMM precipitation radar," *J. Appl. Meteorol.*, vol. 39, no. 12, pp. 2053–2070, Dec. 2000.
[49] E. N. Anagnostou, "Overview of overland satellite rainfall estimation for hydro-meteorological applications," *Surveys Geophys.*, vol. 25, no. 5/6, pp. 511–537, Nov. 2004.
[50] M. Grecu, W. S. Olson, and E. N. Anagnostou, "Retrieval of precipitation profiles from multiresolution, multifrequency active and passive microwave observations," *J. Appl. Meteorol.*, vol. 43, no. 4, pp. 562–575, Apr. 2004.
[51] A. Mugnai, H. J. Cooper, E. A. Smith, and G. J. Tripoli, "Simulation of microwave brightness temperatures of an evolving hail storm at SSM/I frequencies," *Bull. Amer. Meteorol. Soc.*, vol. 71, no. 1, pp. 2–13, Jan. 1990.
[52] J. Vivekanandan, J. Turk, and V. N. Bringi, "Ice water path estimation and characterization using passive microwave radiometry," *J. Appl. Meteorol.*, vol. 30, no. 10, pp. 1407–1421, Oct. 1991.
[53] C. Kummerow, W. Olson, and K. Giglio, "The status of the Tropical Rainfall Measuring Mission (TRMM) after two years in orbit," *J. Appl. Meteorol.*, vol. 39, no. 12, pp. 1965–1982, Dec. 2000.
[54] L. Chiu, D.-B. Shin, and J. Kwaitkowski, "Surface rainfall from satellite algorithms," in *Earth Science Satellite Remote Sensing*, vol. I, J. Qu, W. Gao, M. Kafatos, R. E. Murphy, and V. V. Salomonson, Eds. Berlin, Germany: Springer-Verlag, 2006, pp. 317–336.
[55] M. S. Narayanan *et al.*, "Validation of TRMM merge daily rainfall with IMD rain gauge analysis over Indian land mass," Space Appl. Centre, Ahmedabad, India, Tech. Rep., 2005.
[56] E. Ebert, J. E. Janowiak, and C. Kidd, "Comparison of near real-time precipitation estimates from satellite observations and numerical models," *Bull. Amer. Meteorol. Soc.*, vol. 88, no. 1, pp. 47–64, Jan. 2007.
[57] H. Rahman and D. Sengupta, "Preliminary comparison of daily rainfall from satellites and Indian gauge data," Centre Atmos. Ocean. Sci., Indian Inst. Sci., Bangalore, India, CAOS Tech. Rep. 2007AS1., 2007.
[58] G. Villarini and W. F. Krajewski, "Evaluation of the research version TMPA three-hourly 0.250×0.250 rainfall estimates over Oklahoma," *Geophys. Res. Lett.*, vol. 34, no. 5, Mar. 2007, Art. ID. L05402.
[59] Y. Tian *et al.*, "Component analysis of error in satellite-based precipitation estimates," *J. Geophys. Res.*, vol. 114, no. D24, Dec. 2009, Art. ID. D24101.
[60] M. R. P. Sapiano and P. A. Arkin, "An intercomparison and validation of high-resolution satellite precipitation estimates with 3-hourly gauge data," *J. Hydrometeorol.*, vol. 10, no. 1, pp. 149–166, Feb. 2009.
[61] S. H. Rahman, D. Sengupta, and M. Ravichandran, "Variability of Indian summer monsoon rainfall in daily data from gauge and satellite," *J. Geophys Res.*, vol. 114, no. D17, Sep. 2009, Art. ID. D17113.
[62] S. Nair, G. Srinivasan, and R. Nemani, "Evaluation of multi-satellite TRMM derived rainfall estimates over a western state of India," *J. Meteorol. Soc. Jpn.*, vol. 87, no. 6, pp. 927–939, Dec. 2009.
[63] H. Feidas, "Validation of satellite rainfall products over Greece," *Theor. Appl. Climatol.*, vol. 99, no. 1/2, pp. 193–216, Jan. 2010.
[64] B. J. Sohn, H. J. Han,and E. K. Seo, "Validation of satellite-based high-resolution rainfall products over the Korean Peninsula using data from a dense rain gauge network," *J. Appl. Meteorol. Climatol.*, vol. 49, no. 4, pp. 701–714, Apr. 2010.
[65] Y. Shen, A. Xiong, Y. Wang, and P. Xie, "Performance of high-resolution satellite precipitation products over China," *J. Geophys. Res.*, vol. 115, no. D2, Jan. 2010, Art. ID. D02114.
[66] D. C. Buarque, R. C. D. de Paiva, R. T. Clarke, and C. A. B. Mendes, "A comparison of Amazon rainfall characteristics derived from TRMM, CMORPH and the Brazilian national rain gauge network," *J. Geophys. Res.*, vol. 116, no. D19, Oct. 2011, Art. ID. D19105.
[67] M. O. Karaseva, S. Prakash, and R. M. Gairola, "Validation of high-resolution TRMM 3B43 precipitation product using rain gauge measurements over Kyrgyzstan," *Theor. Appl. Climatol.*, vol. 108, no. 1/2, pp. 147–157, Apr. 2012.
[68] M. N. Islam and H. Uyeda, "Comparison of TRMM 3B42 products with surface rainfall over Bangladesh," in *Proc. IEEE IGARSS*, Seoul, Korea, Jul. 25–29, 2005, pp. 4112–4115.
[69] P. Xie *et al.*, "A gauge-based analysis of daily precipitation over East Asia," *J. Hydrometeorol.*, vol. 8, no. 3, pp. 607–627, Jun. 2007.
[70] A. Yatagai, P. Xie, and A. Kitoh, "Utilization of a new gauge-based daily precipitation dataset over monsoon Asia for validation of the daily precipitation climatology simulated by the MRI/JMA 20-km-mesh AGCM," *SOLA*, vol. 1, pp. 193–196, 2005.
[71] V. Kumar, and T. N. Krishamurti, "Improved seasonal precipitation forecasts for the Asian monsoon using 16 atmosphere-ocean coupled models: Climatology," *J. Clim.*, vol. 25, no. 1, pp. 39–64, Jan. 2012.
[72] A. Yatagai, T. N. Krishnamurti, V. Kumar, A. K. Mishra, and A. Simon, "Use of APHRODITE rain gauge-based precipitation and TRMM 3B43 products for improving asian monsoon seasonal precipitation forecasts by the superensemble method," *J. Clim.*, vol. 27, no. 3, pp. 1062–1069, Feb. 2014.
[73] G. J. Huffman, R. F. Adler, B. Rudolf, U. Schneider, and P. R. Keehn, "Global precipitation estimates based on a technique for combining satellite-based estimates, rain gauge analysis, and NWP model precipitation information," *J. Clim.*, vol. 8, no. 5, pp. 1284–1295, May 1995.
[74] G. J. Huffman, "Estimates of root-mean-square random error for finite samples of estimated precipitation," *J. Appl. Meteorol.*, vol. 36, no. 9, pp. 1191–1201, Sep. 1997.
[75] M. Rajeevan and J. Bhate, "A high resolution daily gridded rainfall dataset (1971–2005) for meso-scale meteorological studies," *Curr. Sci.*, vol. 96, no. 4, pp. 558–562, Feb. 2009.
[76] C. Schumacher and R. A. Houze, "Comparison of radar data from the TRMM satellite and Kwajalein oceanic validation site," *J. Appl. Meteorol.*, vol. 39, no. 12, pp. 2151–2164, Dec. 2000.
[77] T. Kozu, T. Kawanishi, K. Oshimura, M. Satake, and H. Kumagai, "TRMM precipitation radar: Calibration and data collection strategies," in *Proc. IEEE IGARSS, Surf. Atmos. Remote Sens.—Technol., Data Anal. Interpretation*, 1994, vol. 2214, pp. 2215–2217.

[78] A. Aghakouchak and A. Mehran, "Extended contingency table: Performance metrics for satellite observations and climate model simulations," *Water Resour. Res.*, vol. 49, no. 10, pp. 7144–7149, Oct. 2013.
[79] G. J. Ciach, W. F. Krajewski, and G. Villarini, "Product error driven uncertainty model for probabilistic quantitative precipitation estimation with NEXRAD data," *J. Hydrometeorol.*, vol. 8, no. 6, pp. 1325–1347, Dec. 2007.
[80] G. Villarini, W. F. Krajewski, G. J. Ciach, and D. L. Zimmerman, "Product—Error—Driven generator of probable rainfall conditioned on WSR-88D precipitation estimates," *Water Resour. Res.*, vol. 45, no. 1, Jan. 2009, Art. ID. W01404.
[81] Y. Tian *et al.*, "Modeling errors in daily precipitation measurements: Additive or multiplicative?" *Geophys. Res. Lett.*, vol. 40, no. 10, pp. 2060–2065, May 2013.
[82] G. J. Huffman *et al.*, "The global precipitation climatology project (GPCP) combined precipitation dataset," *Bull. Amer. Meteorol. Soc.*, vol. 78, no. 1, pp. 5–20, Jan. 1997.
[83] Y. Tian, and C. D. Peters-Lidard, "A global map of uncertainties in satellite-based precipitation measurements," *Geophys. Res. Lett.*, vol. 37, no. 24, Dec. 2010, Art. ID. L24407.
[84] M. Winchell, H. V. Gupta, and S. Sorooshian, "On the simulation of infiltration-and saturation excess runoff using radar-based rainfall estimates: Effects of algorithm uncertainty and pixel aggregation," *Water Resour. Res.*, vol. 34, no. 10, pp. 2655–2670, Oct. 1998.
[85] M. Borga, E. N. Anagnostou, and E. Frank, "On the use of real-time radar rainfall estimates for flood prediction in mountainous basins," *J. Geophys. Res.*, vol. 105, no. D2, pp. 2269–2280, Jan. 2000.
[86] F. Hossain, E. N. Anagnostou, M. Borga, and T. Dinku, "Hydrological model sensitivity to parameter and radar-rainfall estimation uncertainty," *Hydrol. Processes.*, vol. 18, no. 17, pp. 3277–3299, Dec. 2004.
[87] A. K. Guetter, K. P. Georgakakos, and A. A. Tsonis, "Hydrologic applications of satellite data: 2. Flow simulation and soil water estimates," *J. Geophys. Res.*, vol. 101, no. D21, pp. 26 527–26 538, Nov. 1996.
[88] J. Willmott, "On the validation of model," *Phys. Geogr.*, vol. 2, no. 2, pp. 184–194, Jul. 1981.
[89] A. AghaKouchak, A. Mehran, H. Norouzi, and A. Behrangi, "Systematic and random error components in satellite precipitation data sets," *Geophys. Res. Lett.*, vol. 39, no. 9, May 2012, Art. ID. L09406.
[90] S. Prakash, V. Sathiyamoorthy, C. Mahesh, and R. M. Gairola, "An evaluation of high-resolution multisatellite rainfall products over the Indian monsoon region," *Int. J. Remote Sens.*, vol. 35, no. 9, pp. 3018–3035, May 2014.
[91] D. Kavetski, G. Kuczera and S. W. Franks, "Bayesian analysis of input uncertainty in hydrological modeling: Application," *Water Resour. Res.*, vol. 42, no. 3, Mar. 2006, Art. ID. W03408.
[92] R. Krzyzstofowicz, "The case for probabilistic forecasting in hydrology," *J. Hydrol.*. vol. 249, no. 1–4, pp. 2–9, Aug. 2001.
[93] L. Jiangnan, Z. Yanping, L. Fangzhou, G. Feiyun, and L. Weibiao, "The structural characteristics of precipitation in Asian-Pacific's three monsoon regions measured by tropical rainfall measurement mission," *Acta Oceanol. Sin.*, vol. 33, no. 3, pp. 111–117, Mar. 2014.
[94] J. Indu and D. N. Kumar, "Evaluation of TRMM PR sampling error over a sub tropical basin using bootstrap technique," *IEEE Trans. Geosci. Remote Sens.*, vol. 52, no. 11, pp. 6870–6881, Nov. 2014.
[95] R. Meneghini and D. Atlas, "Simultaneous ocean cross-section and rainfall measurements from space a nadir-looking radar," *J. Atmos. Ocean. Technol.*, vol. 3, no. 3, pp. 400–413, Sep. 1986.
[96] R. A. Houze, S. Brodzik, C. Schumacher, S. E. Yuter, and C. R. Williams, "Uncertainties in oceanic radar rain maps at Kwajalein and implications for satellite validation," *J. Appl. Meteorol.*, vol. 43, no. 8, pp. 1114–1132, Aug. 2004.
[97] J. Indu and D. N. Kumar, "Copula based modeling of TRMM TMI brightness temperature with rainfall type," *IEEE Trans. Geosci. Remote Sens.*. vol. 52, no. 8, pp. 4832–4845, Aug. 2014.
[98] P. E. Kirstetter *et al.*, "Comparison of TRMM 2A25 products version 6 and version 7 with NOAA/NSSL ground radar-based National Mosaic QPE," *J. Hydrometeorol.*, vol. 14, no. 2, pp. 661–669, Apr. 2012.
[99] A. Devasthale, and H. Grassl, "A daytime climatological spatio-temporal distribution of high opaque ice cloud classes over the Indian summer monsoon region from 25-year AVHRR data," *Atmos. Chem. Phys.*, vol. 9, no. 12, pp. 4185–4196, Jun. 2009.
[100] F. Galton, "The geometric mean in vital and social statistics," *Proc. R. Soc. Lond.* vol. 29, pp. 365–367, 1879.
[101] P. D. Gingerich, "Arithmetic or geometric normality of biological variation: An empirical test of theory," *J. Theor. Biol.*, vol. 204, no. 2, pp. 201–221, May 2000.

J. Indu received B.Tech degree in civil engineering from the Mar Athanasius College of Engineering, Kerala, India in 2004 with university third rank, M.Tech degree in geoinformatics from Indian Institute of Technology Kanpur, Kanpur, India, in 2008 and the Ph.D. degree from the Indian Institute of Science (IISc), Bangalore, India, in 2015.

She worked as a Research Associate with the Department of Civil Engineering, IISc. She is currently working as an Assistant Professor, Department of Civil Engineering, Indian Institute of Technology Bombay, Mumbai, India. Her research interests include microwave remote sensing, uncertainty modeling, and nowcasting of precipitation.

D. Nagesh Kumar received the Ph.D. degree from the Indian Institute of Science (IISc), Bangalore, India, in 1992.

He was a Boyscast Fellow with the Utah Water Research Laboratory, Utah State University, Logan, UT, USA, in 1999. He has been a Professor with the Department of Civil Engineering, IISc, since May 2002. He is also the Chairman, Centre for Earth Sciences, IISc. Earlier, he was with the IIT, Kharagpur, India, and National Remote Sensing Centre, Hyderabad, India. His research interests include climate hydrology, climate change, water resource systems, ANN, evolutionary algorithms, fuzzy logic, MCDM, and remote sensing and GIS applications in water resource engineering. He is the coauthor of two text books entitled *Multicriterion Analysis in Engineering and Management* (PHI) and *Floods in a Changing Climate: Hydrologic Modeling* (Cambridge University Press). He has published more than 160 papers including 88 in peer reviewed journals.